**Contributing Editor: Randall Hay**

Author Manuscript

**Bottom up vs reactive sintering of Al₂O₃-YAG-YSZ composites via one or three-phase nanoparticles (NPs). Bottom up processing wins this time.**

Nathan J. Taylor, Sandra Stangeland-Molo, and Richard M. Laine*

Department of Materials Science and Engineering, University of Michigan, Ann Arbor, MI

48109-2136, email: talsdad@umich.edu

## Abstract

The bottom up approach describes the synthesis of bulk materials from the finest possible length scales to obtain the best global properties. This approach was adapted to the synthesis of multi-phase ceramic composites produced from metal oxides produced by liquid-feed flame spray pyrolysis (LF-FSP). The effect of length scale of mixing was tested through two processing schemes, mixed single metal-oxide nanopowders (NPs) and nanocomposite NPs having the desired composition within single particles. For the $Al_2O_3$-$Y_2O_3$-$ZrO_2$ ternary system, composites prepared from nanostructured nanoparticles sinter to finer grain sizes (<410 nm) at equivalent densities of 95 %TD than those prepared from mixed nanoparticle processing. These contrast with our previous studies in this area where mixed NP processing gave the best or equivalent results.

The nanocomposite NPs produced in this study exhibit novel nanostructures with three phases contained within single particles < 26 nm average particle size (APS). This nanostructure may directly explain the enhanced sintering of the nanocomposite NPs and may provide an impetus for future synthesis of similarly structured NPs.

## Introduction

The bottom up concept of materials processing argues that mixing of individual components at atomic or molecular levels offers the potential to minimize diffusion distances during processing that should minimize processing times, temperatures and final grain sizes thereby optimizing final global properties.[1-8] This concept gave rise to intense research in sol-gel (chimie douce) and precursor processing.[9-12] However, the universality of this approach conflicts with other processing mandates. For example, traditional processing often requires final products that exhibit closed porosity considered to be ca. 95 % of theoretical density and coincident high phase purity.

We recently explored using single-phase (or nanocomposite) mixed-metal nanoparticles (NPs) as starting points for bottom up processing of dense ceramic monoliths and thin films.[13-19] For comparative purposes we also used ball milled (BM) mixtures of NPs of the same global composition. The scale of mixing is nearly atomic in the first case with typical diffusion lengths of 5-30 nm. In the BM case, average diffusion lengths are equal to agglomerate sizes of 100-800 nm.

It was anticipated that single-phase systems would permit lower temperature processing and/or provide superior densification rates and finer final grain sizes. However, we find that sintering $\alpha$-$Al_2O_3$/$MAl_2O_4$ (M = Mg, Co, Ni) composites BM mixtures of t-$Al_2O_3$ NPs with spinel $MAl_2O_4$ NPs gave dense composites with microstructures identical to those from single phase (atomically mixed) spinel NPs.[13,15] Furthermore, reactive sintering of BM $3Y_2O_3$:$5Al_2O_3$ NPs produced higher densities and finer grain sizes in YAG tubes than obtained by single phase $Y_3Al_5O_{12}$ composition NPs.[16]

In a single-phase material, grain boundary migration can be accommodated by diffusion across the grain boundary or by a dislocation climb and glide mechanism for low-angle boundaries. In a multi-phase system in which a secondary phase exists as a discrete insoluble phase, grain boundary migration can be suppressed through Zener pinning.[20] However, this treatment does not necessarily apply in the case that the secondary phase has a similar grain size to the primary phase or in the case that there is solubility between the two phases. In the case of a solute or impurity phase at a grain boundary, grain boundary migration can be suppressed through the solute drag effect, in which grain boundary mobility is governed by diffusion of the solute back to the grain boundary. If the boundary velocity is high enough, the grain boundary can break away from the solute cloud, in which case boundary migration identical to that of the single-phase case. In a multi-phase material of dissimilar materials, equivolumetric four-phase composites would theoretically provide complete isolation in 3D space, i.e. a grain of one material should not share a grain boundary with a grain of the same phase.[23] In this case, grain boundaries cannot migrate by diffusion of like atoms across grain boundaries, and longer diffusion distances can be required along grain boundaries which limits boundary mobility.[23] This provides part of the motivation for the work described here with the understanding that significant solubility exists within the $Al_2O_3$-$Y_2O_3$-$ZrO_2$ system.

Starting from YAG/$\alpha$-Al$_2$O$_3$ composite NP systems we produced composites with a third phase, Y$_2$O$_3$ stabilized c-ZrO$_2$. Previously, LF-FSP core-shell ZrO$_2$-Al$_2$O$_3$ powders were shown to sinter to fully dense composites at 1120° C with AGSs < 200 nm.[14] The studies described here sought to test: (1) the pinning effect of a third phase on grain size, (2) the effect of a phase with a lower sintering temperature, and (3) the effect of the so-called "bottom-up" approach to composite processing. Here we refer to the composites in terms of their vol% (and mol%) YSZ fraction.

Several groups have produced eutectic composites in the Al$_2$O$_3$-YAG-YSZ system.[24-28] Eutectic composites are typically produced as prospective high-temperature structural materials. A few examples of powder processed Al$_2$O$_3$-YAG-YSZ or AYZ composites have been reported. Palmero et al.[29] synthesized AYZ composites from YCl$_3$ and ZrCl$_4$ decomposition on nanosized transition Al$_2$O$_3$ NPs of 90 Al$_2$O$_3$- 5 YAG-5 vol% YSZ, 60 Al$_2$O$_3$- 20 YAG-20 vol % YSZ, and 34 Al$_2$O$_3$-33 YAG-33 vol % YSZ. In sintering 34:33:33 vol % slip cast composites, they demonstrated AGS < 500 nm after 3 h at 1500° C at 98 % TD.

Oelgardt et al.[30] synthesized AYZ composites at the same compositions as reported here by milling < 300 nm commercially available powders of Al$_2$O$_3$-Y$_2$O$_3$-Al$_2$O$_3$ (AYZ) and Al$_2$O$_3$-YAG-YSZ (YAG-AZ) achieving 95 % TD after sintering 1 h at 1500° C with AGSs of 550 nm for Al$_2$O$_3$, 560 nm for YAG, and 460 nm for YSZ.

The YAG-AZ produced by Oelgardt et al sintered to 98 % TD after 1 h at 1500° C with AGSs of 640 nm for Al$_2$O$_3$, 780 nm for YAG, and 500 nm for YSZ. Kim and Kriven[31] synthesized 34:33:33 vol % AYZ composites from NPs produced by the steric entrapment method. Samples sintered to full density after 3 h at 1550 ° C with AGSs > 1 μm.

In this study, the nanocomposite NP processing method represents bottom up processing, where the length scale of mixing is within the average particle size, APS, or < 30 nm. At best, the mixed (BM) NP approach gives a length scale of mixing within the volume of three adjacent particles of each separate material. However, perfect mixing is unlikely, and the length scale of mixing is likely on the order of agglomerate size, which can vary from 100-800 nm.

Liquid-feed flame spray pyrolysis (LF-FSP) is a combustion synthesis technique providing high throughput (100 g/h) powder production ideal for processing studies.[13-19] In LF-FSP, metalloorganic precursors are dissolved in alcohol solutions. These precursor solutions are pumped through a nozzle, where they are aerosolized with O$_2$ and ignited and combusted in a 1.5 m long quartze tube at temperatures of 900-1400°C and quenched to$\approx$ 300 °C in < 100 msec

thereafter. The powders are collected in electrostatic precipitators. Typical LF-FSP powers have specific surface areas (SSAs) of 30-120 $m^2$/g and corresponding primary particle sizes of 100-20 nm.[13-19]

As noted just above, the motivation for the current work is to extend our results on reactive sintering of BM mixtures of NPs to three components and compare results with a "bottom up" approach using atomically mixed NPs of the same global composition. The long-term objective of this and previous studies is to detail the various aspects of NP sintering behavior as a function of length scale of mixing to identify critical points in the process leading to an improved under-standing of process variables that control densification, grain growth, pore evolution and to use this knowledge to advantage in the design of optimal sintering methods. There are limitations to this objective, namely that particle size distributions, pore size distributions, green density and additional factors play a large role in sintering dense, homogeneous compacts.

Experimental

Precursors Yttrium propionate, $(CH_3CH_2CO_2)_3Y$, was used as a precursor to $Y_2O_3$. Alumatrane, $[N(CH_2CH_2O)_3Al]$, was used a precursor to $Al_2O_3$. Yttrium propionate was pre-pared by the dissolution of $Y_2(CO_3)_3$ or $Y_2O_3$ (PIDC, Ann Arbor, MI) in propionic acid (Acros Organics, Geel, Belgium). Approximately 200 g (0.885 mol $Y_2O_3$) of starting material and 1 L (13.3 mol) of propionic acid was placed into a 3 L round bottom flask with magnetic stirring un-der dry $N_2$.

The reaction was heated to 120° C for 10 h, distilling off water. Upon full dissolution of the starting material into the propionic acid to produce a yellow liquid, the reaction was heated 145° C and excess acid was distilled off. The reaction was cooled, and yttrium propionate precipitated from the supersaturated solution. The synthesis of alumatrane is well described elsewhere.[13] Zir-conium isobutyrate was used as a precursor to $ZrO_2$. Zirconium isobutyrate was produced from the reaction of isobutyric acid with zirconium basic carbonate at 130° C. Dried zirconium basic carbonate, $Zr(OH)_2CO_3 \bullet ZrO_2$, (200 g, 0.49 mol) was added to a 1 L round bottom flask with 600 mL (6.6 mol) and the reaction was heated to 140° C for 5 h until all of the zirconium basic carbonate was dissolved. Isobutyric anhydride was added and the reaction was continued for 8 h at 155° C until a dark brown solution was obtained. The obtained zirconium isobutyrate had a TGA ceramic yield of 42.0%, which means the precursor likely had a formula of $[(Me_2CHCO_2)_2(OH)Zr]O[Zr(OH)(O_2CCHMe_2)]$, with a theoretical ceramic yield of 42.4%.

LF-FSP Precursors were dissolved at the desired molar ratio in anhydrous ethanol at < 3 wt% ceramic loading. Precursor solutions were aerosolized with $O_2$ in the nozzle combusted at standard LF-FSP conditions.

Powder processing Approximately 20 g of powder was ball milled with 99.5% $Al_2O_3$ media in ethanol for 24 h with 2 wt% bicine [$HO_2CCH_2N(CH_2CH_2OH)_2$]. Powders were then ultrasonicated for 20 minutes at 100W of power with a Vibracell VC-505 ultrasonic horn (Sonics & Materials, Newtown, CT). The powders were settled for 24 h, after which the remaining suspended powder was decanted. For mixtures of different powders, powders were first dispersed in ethanol and settled for 24 h prior to milling to account for any differences in settling rate. The powders were dried, ground, and sieved through 79 μm mesh. The powders were dispersed in ethanol with 4 wt% PEG 3400 as binder and ultrasonicated for 20 minutes at 100W of power. The powders were dried, ground, and sieved through 30 μm mesh. The powders were pressed at 14 MPa and cold isostatically pressed at 200 MPa.

X-ray diffraction (XRD) Powder X-ray diffraction was performed on a Rigaku rotating anode diffractometer (Rigaku USA, The Woodlands, TX) at 40 kV and 100 mA. Typical continuous scan ranges were from 10-70 ° 2θ at 2°/min with a 0.02° interval. XRD patterns were analyzed using JADE 2010. Rietveld refinements were conducted within JADE.

Scanning electron microscopy (SEM) SEM was performed using a FEI Nova Nanolab dualbeam SEM/FIB or FEI Quanta 200 SEM/FIB (FEI Corporation, Hillsboro, OR). Typical accelerating voltages were 5-20 kV, depending on sample conditions. Powder samples (50 mg) were ultrasonicated in 20 mL of ethanol and dropped onto SEM sample stubs. Pellets were mounted on sample stubs with copper tape.

Transmission electron microscopy (TEM) TEM was performed using a JEOL 3011 HREM (JEOL Ltd., Tokyo, Japan) at 300 kV. Powder (10 mg) was dispersed in 20 mL ethanol and wicked through a 400 mesh carbon coated copper grid.

Thermogravimetric analysis/differential thermal analysis (TGA/DTA) TGA/DTA was performed on a TA Instruments Q600 TGA/SDT (TA Instruments, New Castle, DE). Precursor ceramic yields were determined by experimental runs at 10 °C/min to 1000 °C. Thermal behavior of ceramic particles or pellets was characterized by sample runs at 10 °C/min to 1400 °C. All experiments were performed with dry air flowing at 60 mL/min.

Specific surface area (SSA) analyses were run using a ASAP 2020 sorption analyzer (Micromeritics, Norcross, GA). Samples were degassed for 8 h at 400 ℃ under vacuum. An 11 point BET method analysis was conducted on 200 mg samples at relative pressures of 0.05-0.35. Nitrogen was used as the adsorbate gas and analysis was conducted in liquid nitrogen. APSs were derived from BET SSAs per Eq. **1**, where ρ is the particle density.

$$d = \frac{6}{(SSA)*\rho} \ (1)$$

Dilatometry Dilatometry was conducted with a Dilatronic II single pushrod dilatometer (Theta Industries, Port Washington, NY). Linear displacement was observed by a linear variable differential transformer (LVDT) and recorded by a custom LabView program. Constant heating rate experiments were conducted from room temperature to 1500 ℃ with a 10℃/min ramp rate in static air.

Vickers microhardness Microhardness measurements were made using a Clark CM-400AT equipped for Vickers hardness measurements. All measurements were taken at a load of 500 g. Values given are at least an average of ten separate indentation sites.

## Results and Discussion

The major objective of work reported here is to test the effect of length scale of mixing on the production of fine-grained composites from mixed NP and nanocomposite NP routes. Within this objective, we are specifically interested in how the length scale of mixing in the initial mixture affects the sintering behavior and the final microstructure of the composite. A secondary objective is to determine if a third phase leads to a reduction in grain size due to the aforementioned pinning effect. In the following, we begin with characterization of the as-produced NPs, then discuss their sintering behavior and final microstructures along with preliminary hardness measurements. Sintering efforts targeted densities of 95 %TD, which represents a starting point for HIPing studies.

Powder characterization

All NPs were produced under standard LF-FSP conditions. Table **1** lists the three compositions studied in both vol% and mol% of the final composite phases. All compositions will be reported in both vol % and mol % YSZ. Complete compositions are presented in Table **1**.

Figure **1** shows an SEM micrograph of 15 vol% (10 mol%) YSZ as-produced nanocomposite NPs. The powders are typical of LF-FSP synthesis with no fraction of larger particles. Table **2** shows the BET SSAs for each powder and a corresponding APS. BET SSAs are typical for LF-FSP NPs, and the single metal oxide particles have similar APSs (20-30 nm) as the nanocomposite NPs.

Figure **2** shows the XRD patterns for the as-produced nanocomposite NPs. Cubic yttria stabilized $ZrO_2$ is the primary phase visible by XRD, along with hexagonal $YAlO_3$ and $\delta^*$-$Al_2O_3$. Hexagonal $YAlO_3$ is a common intermediate phase in the synthesis of YAG[32], and $\delta^*$-$Al_2O_3$ is the most common phase in LF-FSP produced $Al_2O_3$ NPs.[17,29] The phases indicated by XRD match the corresponding powder diffraction files for equilibrium crystal structures. The relatively strong reflections of the YSZ phase are attributed to the high scattering intensity of the YSZ phase.

For the mixed nanoparticle case, $ZrO_2$ is a mixture of 48 wt % monoclinic $ZrO_2$ and 52 wt % tetragonal $ZrO_2$. $Y_2O_3$ is a mix of 10 wt % monoclinic and 90 wt % cubic phases. $Al_2O_3$ is a mixture of transition $Al_2O_3$ phases, at 57 wt % $\delta^*$-$Al_2O_3$, 30 wt % $\delta$-$Al_2O_3$, and 15 wt % $\gamma$-$Al_2O_3$.

Figure **3** shows a TEM of a nanocomposite nanoparticle with inset close-up micrographs of the three major crystalline regions within the particle. Fast Fourier transforms (FFTs) of each crystalline region provide the lattice spacings given on the inset micrographs. The crystalline region with a spacing of 0.30 nm corresponds to the (111) c-YSZ planar spacing, the region with a spacing of 0.53 nm corresponds to the (002) hexagonal $YAlO_3$ spacing, and the region with a spacing of 0.23 nm corresponds to the (132) $\delta^*$-$Al_2O_3$. The lattice spacings in this figure match with the phases observed by XRD. FFTs were used in lieu of selected area electron diffraction (SAED) due to the difficulty in producing usable SAED patterns from such small regions. The $\delta^*$-$Al_2O_3$ inset region does match with the (132) plane spacing by FFT, but it is difficult to resolve. An additional spot on the FFT gives a planar spacing of 0.38 nm, which corresponds to the (021) $\delta^*$-$Al_2O_3$ planar spacing. Given these are the only three phases present by XRD, it is likely this region corresponds to the $\delta^*$-$Al_2O_3$ phase. In addition, many other particles were observed having multiple crystalline regions corresponding to different phases, supporting a multiphase, composite particle morphology. Figure **4** shows another particle with two clear crystalline regions.

FFTs give a lattice spacing for the left region of 0.53 nm, consistent with the hexagonal $YAlO_3$ (002) spacing, and secondary FFT points in the same orientation at 0.26 nm correspond to the (004) spacing. In the other crystalline region, FFTs give a lattice spacing of 0.30 nm, consistent with the c-YSZ (111) plane. Figure **5** provides four more particles with similar morphology. These TEMs provide a strong set of examples of nanocomposite nanoparticles, which is a novel finding for single step gas-phase particle generation.

This novel result has implications beyond the composite processing presented here. Synthesis of targeted two-phase or Janus particles has been extensively investigated for applications such as self-assembly and combinations of materials with different optical or magnetic properties on the nanoscale.[34,35] These results suggest flame spray pyrolysis may be a way to synthesize some of these multi-phase structures without extensive processing usually required.

Dilatometry

Figure **6** shows the dilatometry traces for both nanocomposite NP and mixed NP processing approaches. The plateaus seen in the dilatometry traces may correspond to phase transformations. It

is difficult to separate out individual phase transformations, as hexagonal $YAlO_3$ typically transforms into both YAP and YAM, as does $Y_2O_3 + Al_2O_3$. Perovskite-$YAlO_3$ ($V_m = 37.2$ cm$^3$/mol) reacts with α-$Al_2O_3$ ($V_m = 25.6$ cm$^3$/mol) to form YAG ($V_m = 130.5$ cm$^3$/mol) with the reaction $6YAlO_3 + 2Al_2O_3 \rightarrow 2Y_3Al_5O_{12}$ with a 10% increase in molar volume, which would not be seen as dilatometric shrinkage. This typically occurs in the temperature range of 1000-1250° C.[16] However, hexagonal-$YAlO_3$ ($V_m = 37.2$ cm$^3$/mol) reacts with $Al_2O_3$ to form YAG with a 7% reduction in molar volume in the temperature range 900-1250° C.[17] In addition, the transformation of the transition $Al_2O_3$ phase to α-$Al_2O_3$ also occurs between 1000-1150° C with a 10% reduction in molar volume.[33] The first trend seen is increasing YSZ content is associated with higher densification up to 1500° C. For the nanocomposite NP samples, linear densification goes from 9 to 17% on increasing the YSZ volume fraction from 15 to 32 %. In the mixed NP samples, linear densification goes from 9 to 15% as YSZ volume fraction increases from 15 to 32%. The second trend is that, nanocomposite NP processing provides higher densification up to 1500° C than the mixed NP approach for a given composition in contrast to our previous studies in this area.[14-17]

Final microstructures

Figure **7** shows polished SEM micrographs for all the composites, with AGSs measured for each phase tabulated in Table **3**. Sintering schedules targeted densities of 95 %TD, and all AGSs were taken at samples of similar relative density, 95-97 %TD. Phases can be delineated by Z-contrast, with YSZ appearing white, YAG appearing gray, and α-$Al_2O_3$ appearing black. As dilatometry shows, densification up to 1500°C increases as $ZrO_2$ content increases. As the $ZrO_2$ content increases, lower sintering temperatures were required to reach at least 95% TD as reflected in finer grain sizes.

In relative proportion, YSZ generally has the finest grain sizes, followed by YAG and then $Al_2O_3$. At 32 vol % (23 mol %) YSZ, the AGSs for all three phases are under 410 nm. Although the nanocomposite NP approach leads to finer grain sizes than the mixed NP case, the effect is lessened as $ZrO_2$ content increases. The finest grain sizes here, 410±210 nm, are ≈ 100 nm lower than the finest grain sizes reported in the literature achieved by pressureless sintering. Oelgardt et al.[30] produced (23/26/51) vol % composites at 95 % TD after sintering 1 h at 1500° C with AGSs of 550 nm for $Al_2O_3$, 560 nm for YAG, and 460 nm for YSZ, slightly higher than the grain sizes

reported here. Kim and Kriven[29] produced (33/33/33 vol%) composites with grain sizes 1-7 µm after 1 h of sintering at 1550-1750° C.

<u>Vickers microhardness</u>

Vickers microhardness measurements were taken on samples of each composition and tabulated in Table **4**. They do not vary much with composition with all samples within a 0.6 GPa range. In the accompanying α-$Al_2O_3$/YAG composite paper, we saw significant shifts in hardness with composition, attributed to α-alumina dominating the observed hardness values. Here we do not see the same effect, although the change in vol % $Al_2O_3$ across the three compositions is Δ12 vol %, where it was Δ37 vol % for α-$Al_2O_3$/YAG.

Oelgardt et al obtain hardnesses ranging from 16-19 GPa, for the same composition (23 vol % YSZ composite), slightly above the hardness measured here at equivalent grain sizes obtained by pressureless sintering.[30] Hardness is likely dominated by the α-$Al_2O_3$ volume fraction, which agrees with the hardnesses here that are well above those of YSZ (12.3 GPa) or YAG (13.7 GPa).[17]

Note that the hardness values for both approaches to the same materials are very similar and in part reflect the fact that the Vickers microhardness measurements have indents that are 10 µm or greater and as such, the data average hardness for a large number of grains. Given the statistical deviation in AGSs, the similarities seen are not unexpected, and again are in keeping with previous studies.

The results show in the $Al_2O_3$-$Y_2O_3$-$ZrO_2$ system, nanocomposite NPs sinter to higher densities at lower temperatures giving finer grain sizes than mixed NPs at equivalent densities or 95 %TD, in contrast with our previous studies. In this case, the bottom up approach was the optimal composite processing strategy. In the mixed NP approach, initial phase separation obtained from ball milling gives a minimum separation distance of ~ 40 nm. The maximum phase separation is likely on the scale of the agglomerate size, which could be 100-800 nm. In the nanocomposite NP processing approach, the maximum phase separation distance is less than the APS of 40 nm.

These results imply phase separation on the nanoscale during sintering does have a significant effect on the final microstructure of the composite, despite significant microstructure coarsening. From a different perspective, we can calculate the approximate number of NPs needed to represent the final volume of the three phases in the dense composite using the AGSs and APSs for the nanocomposite NP 32 vol % YSZ composition. Assuming that grains are tetradecahedral,

the volume of a tetradecahedron is given by Equation 2, where *D*, the average grain size, is related to the tetradecahedron edge length, *l*, by the relationship $D = 3l$.[36]

$$V = 8\sqrt{2}l^3 \quad (2)$$

Assuming spherical particles, we find an approximate volume coarsening ratio of 8000. This means for the finest grain sizes obtained here, three adjacent grains of separate phases started from an average of 8000 nanostructured NPs. This number illustrates the novelty of the difference observed between the two processing approaches. The finest grain sizes for YAG-$Al_2O_3$-YSZ in the composites also start with powders < 100 nm, giving a similar volume coarsening ratio from the green body.

Although the intermediate sintering mechanisms are unclear, it is clear that the addition of $ZrO_2$ is important in reducing the grain size, as the grain sizes (410 nm) here are much less than the > 1 μm AGSs obtained for α-$Al_2O_3$/YAG composite. For the nanocomposite NP case, the initial finer length scale of mixing may allow YSZ coalescence which promotes sintering in the 1200-1300° C range leading to higher final densities after the second significant densification regime of 1350-1500° C. Alternatively, the pinning effect of the third phase on the finest length scale, i.e. within the same NP, may become an important factor.

It is important to note that there are many factors affecting sintering that are uncontrolled in this study. Particle size distribution, degree of agglomeration, and pore size distribution in the green compact. Additionally, solid-state reactions within the $Al_2O_3$-$Y_2O_3$-$ZrO_2$ may enhance or be detrimental to overall densification. However, the results here show that for particles that are relatively similar in morphology and particle size, the solid-state reactions that occur during sintering do effect global densification.

## Conclusions

The bottom up approach postulates that best global properties are obtained from synthesis processes that start at the finest possible size. This approach, vis-à-vis the length scale of mixing, was tested here through two processing schemes, mixed single metal-oxide NPs, and nanocomposite NPs have the desired composition within single particles. We find that in the $Al_2O_3$-$Y_2O_3$-$ZrO_2$ ternary system, composites prepared from nanostructured nanoparticles sinter to finer grain sizes at equivalent densities of 95 %TD than those prepared from mixed nanoparticle processing.

These contrast with all our previous studies in this area where mixed NP processing gave the best or equivalent results. As a whole, our studies suggest the preferred processing route is highly dependent upon system specific variables, such as phase transformations and diffusion coefficients within specific phases.

The final microstructures for both processing schemes consist of well-dispersed composite phases. The addition of a $ZrO_2$ phase permits pressureless sintering to dense composites with extremely fine (410 nm) AGSs through $ZrO_2$ sintering or by pinning grain boundary movement of the other phases.

One major finding is clear evidence observed by TEM of nanostructured nanoparticles containing the metastable $YAlO_3$ and $\delta^*$-$Al_2O_3$ phases along with c-YSZ. These are the first LF-FSP ternary phase particles directly observed to have such structure. Nanostructured NPs thus represent a promising avenue for LF-FSP studies, as intra-particle interfaces may give rise to novel properties.

## Acknowledgements

## References

1.  C.M. Lieber, "Nanoscale Science and Technology: Building a Big Future from Small Things "*MRS Bulletin*. **28**, 486-8 (2003).

2.  L. Zhi and K. Mullen, "A bottom-up approach from molecular nanographenes to unconventional carbon materials, "*J. Mater. Chem.*, **18**, 1472-84 (2008).

3.  R. Murugavel, H.G. Walawalkar, M. Dan, H.W. Roesky, and C.N.R. Rao, *Acc. Chem. Res.*, 37, 763-67 (2004).

4.  L. G. Hubert-Pfalzgraf, "To what extent can design of molecular precursors control the preparation of high tech oxides?," *J. Mater. Chem.*, **14**, 3113-23, (2004).

5.  W. Lu and C.M. Lieber, "Nanoelectronics from the bottom up," *Nature Materials*., **6**, 841-850 (2007).

6.  J. Binner and B. Vaidhyanathan, "Processing of Bulk Nanostructured Ceramics," *J. Eur. Ceram. Soc.*, **28**, 1329-39 (2008).
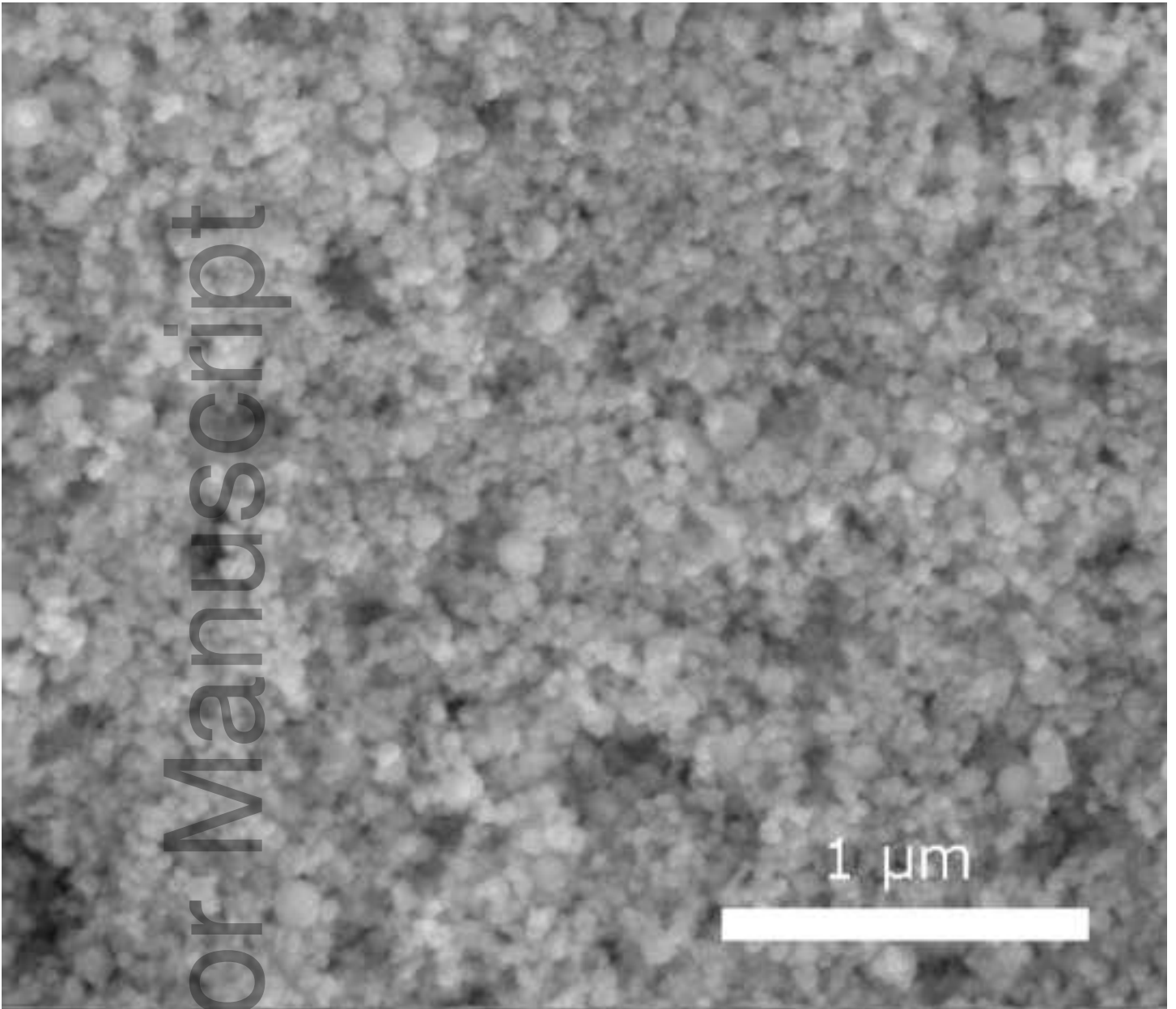
7.  R. Ramaseshan, S. Sundarrajan, R. Jose, and S. Ramakrishna, "Nanostructured ceramics by electrospinning, "*J. App. Phys.* **102** , 111101 (2007*).

8.  S. Komarneni, "Nanocomposites," *J. Mater. Chem.*, **2**, 1219-30 (1992).

9.  C. J Brinker and G. Scherer, Sol-Gel Science, Academic Press, N.Y., N.Y. 1991.

10. J. Livage, M. Henry, and C. Sanchez, "Sol-gel Chemistry of Transition Metal-Oxides," *Prog. in Solid State Chem.*, **18**, 259-341 (1988).

11. R.M. Laine, F. Babonneau, "Preceramic polymer routes to silicon carbide," *Chem. Mat.* **5**, 260-79 (1993).

12. R.M. Laine, A. Sellinger, "Si-containing ceramic precursors," in The Chemistry of Organic Silicon Compounds Vol. 2, Z. Rappoport Y. Apeloig, eds., J. Wiley & Sons Ltd. London, 1998, 2245-310.

13. T. R. Hinklin, J. Azurdia, M. Kim, J. C. Marchal, S. Kumar, and R. M. Laine, "Finding Spinel in all the Wrong Places," *Adv. Mater.*, **20**, 1373–5 (2008).

14. M. Kim and R.M. Laine, "Pressureless Sintering t-zirconia@$\delta$-Al$_2$O$_3$ (54 mol%) Core–Shell NPs at 1120°C Provides Dense t-Zirconia-Toughened $\alpha$-Al$_2$O$_3$ Nanocomposites," *J. Amer. Cer. Soc.*, **93** 709–15 (2010).

15. N. J. Taylor, A. J. Pottebaum, V. Uz, R. M. Laine, "The bottom up approach is not always the best processing method. Dense $\alpha$-Al$_2$O$_3$/NiAl$_2$O$_4$ composites," *Adv. Functional Mater.*, **24**, 3392–98 (2014).

16. N. J. Taylor, R.M. Laine, "Bottom up processing is not always optimal. YAG tubes," *Adv. Functional Mater.*, **24**, 1125-32 (2014).

17. R. M Laine, N. J. Taylor and S. Stangeland-Molo, submitted for publication.

18. J. Marchal, T. John, R. Baranwal, T. Hinklin, and R.M. Laine, "Yttrium aluminum garnet NPs produced by liquid-feed flame spray pyrolysis (LF-FSP) of metalloorganic precursors'" *Chem. Mater.*, **16** 822-31 (2004).

19. T. Hinklin, B. Toury, C. Gervais, F. Babonneau, J.J. Gislason, R.W. Morton, and R.M. Laine, "Liquid-Feed Flame Spray Pyrolysis of Metalloorganic and Inorganic Alumina Sources in the Production of Nanoalumina Powders," *Chem. Mater.*, **16** 21–30 (2004).

20. H. Gleiter, "The mechanism of grain boundary migration," *Acta Metall.*, **5** 565-573 (1969).

21. B. Evans, J. Renner, and G. Hirth, "A few remarks on the kinetics of static grain growth in rocks," *Intl. J Earth Sci.*, **90** 88-103 (2001).

22. E. Nes, N. Ryum, and O. Hunderi, "On the Zener drag," *Acta Metall.*, **33** 11-22 (1985).

23. D. Men and M. L. Mecartney, "Superplasticity and machinability in a four-phase ceramic," *Mater. Res. Bull.*, **47** 1925–31 (2012).

24. A. Larrea, V.M. Orera, R.I. Merino, and J.I. Peña, "Microstructure and mechanical properties of $Al_2O_3$–YSZ and $Al_2O_3$–YAG directionally solidified eutectic plates," *J. European Ceramic Soc*, **25** 1419–29 (2005).

25. H. Su, J. Zhang, J. Yu, L. Liu, and H. Fu, "Rapid solidification and fracture behavior of ternary metastable eutectic $Al_2O_3$/YAG/YSZ in situ composite ceramic," *Materials Science and Engineering: A*, **528** 1967–73 (2011).

26. F. J. Ester, A. Larrea, and R.I. Merino, "Processing and microstructural study of surface laser remelted $Al_2O_3$–YSZ–YAG eutectic plates," *J. Eur. Cer. Soc.*, **31** 1257–68 (2011).

27. J. M. Calderon-Moreno and M. Yoshimura, "$Al_2O_3$–$Y_3Al_5O_{12}$(YAG)–$ZrO_2$ ternary composite rapidly solidified from the eutectic melt," *J. Eur. Cer. Soc.*, **25** 1365–68 (2005).

28. P. B. Oliete, J.I. Peña, A. Larrea, V.M. Orera, J. LLorca, J.Y. Pastor, A. Martín, and J. Segurado, "Ultra-High-Strength Nanofibrillar $Al_2O_3$–YAG–YSZ Eutectics," *Adv. Mater.*, **19** 2313–18 (2007).

29. P. Palmero, G. Pulci, F. Marra, T. Valente. and L. Montanaro, "$Al_2O_3$/$ZrO_2$/$Y_3Al_5O_{12}$ Composites: A High-Temperature Mechanical Characterization," Materials, **8**, 611-24 (2015).

30. C. Oelgardt, J. Anderson, J.G. Heinrich, and G.L. Messing, "Sintering, microstructure and mechanical properties of $Al_2O_3$–$Y_2O_3$–$ZrO_2$ (AYZ) eutectic composition ceramic microcomposites," *J. Europ. Cer. Soc.*, **30** 649–56 (2010).

31. D.-K. Kim and W.M. Kriven, "Processing and Characterization of Multiphase Ceramic Composites Part II: Triplex Composites with a Wide Sintering Temperature Range," *J. Am. Cer. Soc.*, **91** 793–98 (2008).

32. S.-M. Sim, K.A. Keller, and T.-I. Mah, "Phase formation in yttrium aluminum garnet powders synthesized by chemical methods," *J. Mater. Sci.*, **35** 713–17 (2000).

33. I. Levin and D. Brandon, "Metastable Alumina Polymorphs: Crystal Structures and Transition Sequences," *J. Am. Cer. Soc.*, **81** 1995-2012 (1998).

34. D.K. Yi, S.S. Lee, G.C. Papaefthymiou, and J.Y. Ying, "Nanoparticle Architectures Templated by $SiO_2$/$Fe_2O_3$ Nanocomposites," *Chem. Mater.*, **18** 614-619 (2006).
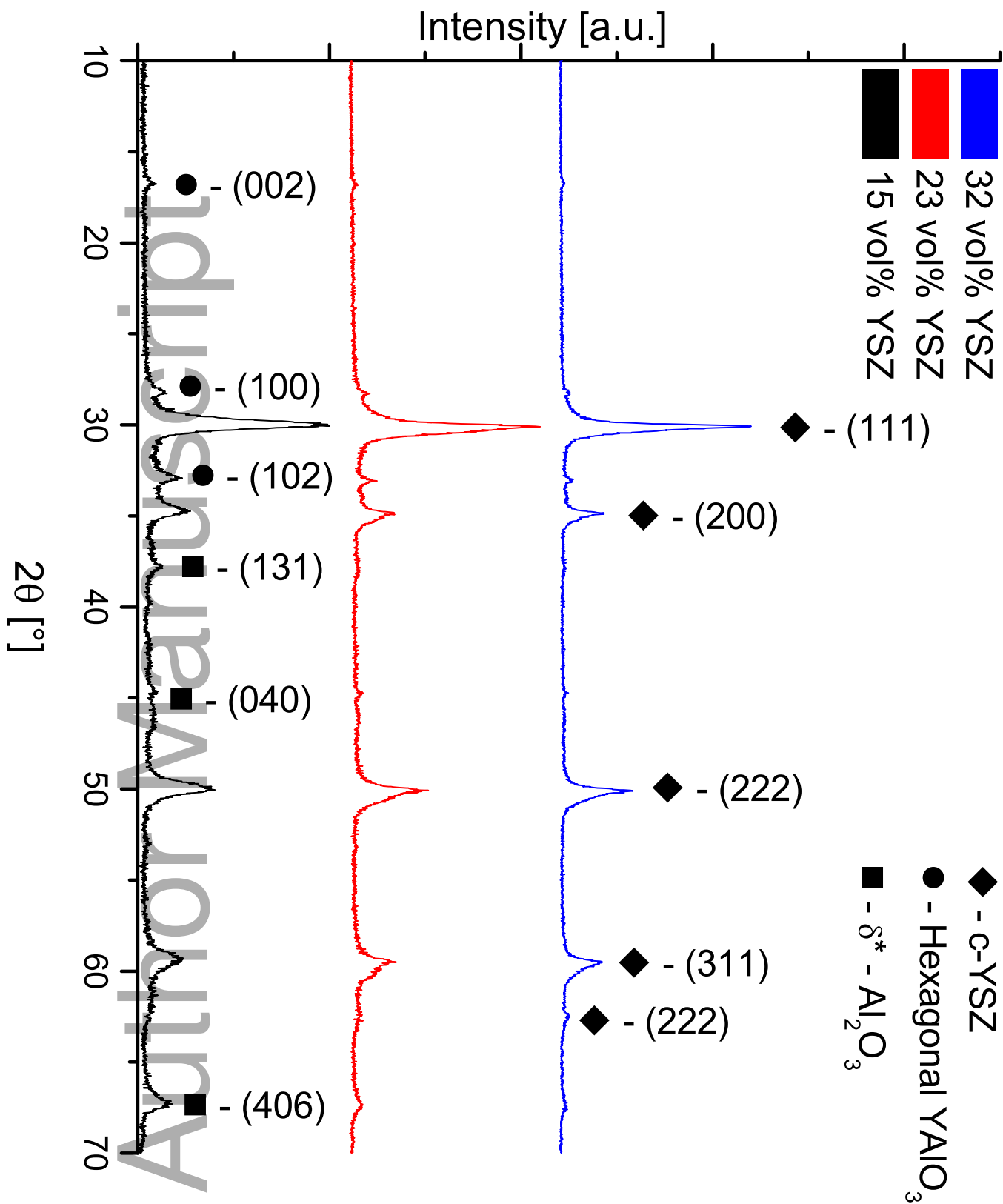
35. A. Perro, S. Reculusa, S. Ravaine, E. Bourgeat-Lami, and E. Duguet, "Design and synthesis of Janus micro- and nanoparticles," *J. Mater. Chem.*, **15** 3745-3760 (2005).

36. M. I. Mendelson, "Average Grain Size in Polycrystalline Ceramics," *J. Amer. Cer. Soc*, **52** 443–446 (1969).
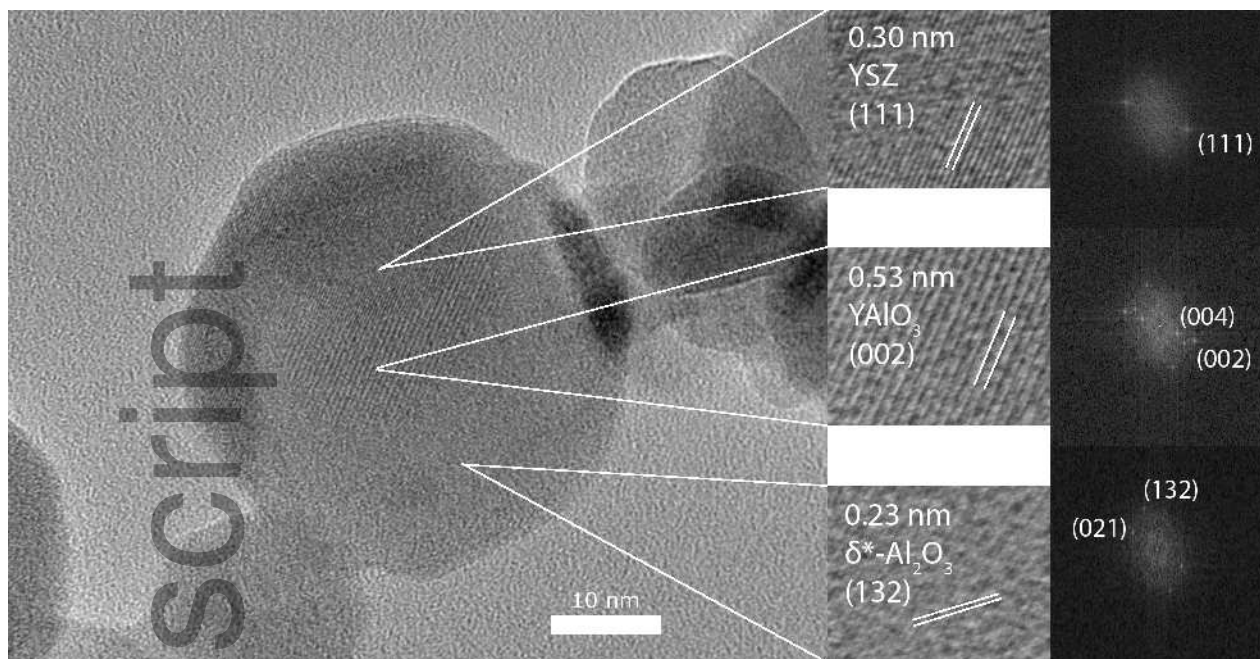
jace_14761_f1.tif

Figure showing XRD patterns with Intensity [a.u.] versus 2θ [°].

Legend:
- 32 vol% YSZ (blue)
- 23 vol% YSZ (red)
- 15 vol% YSZ (black)

- ◆ - c-YSZ
- ● - Hexagonal YAlO$_3$
- ■ - δ* - Al$_2$O$_3$

Black curve peaks: ● - (002), ● - (100), ● - (102), ■ - (131), ■ - (040), ■ - (406)

Blue curve peaks: ◆ - (111), ◆ - (200), ◆ - (222), ◆ - (311), ◆ - (222)

jace_14761_f2.eps

jace_14761_f3.tif

0.30 nm
YSZ
(111)

0.53 nm
YAlO₃
(002)

10 nm

jace_14761_f4.tif

jace_14761_f5.tif

Author Manuscript

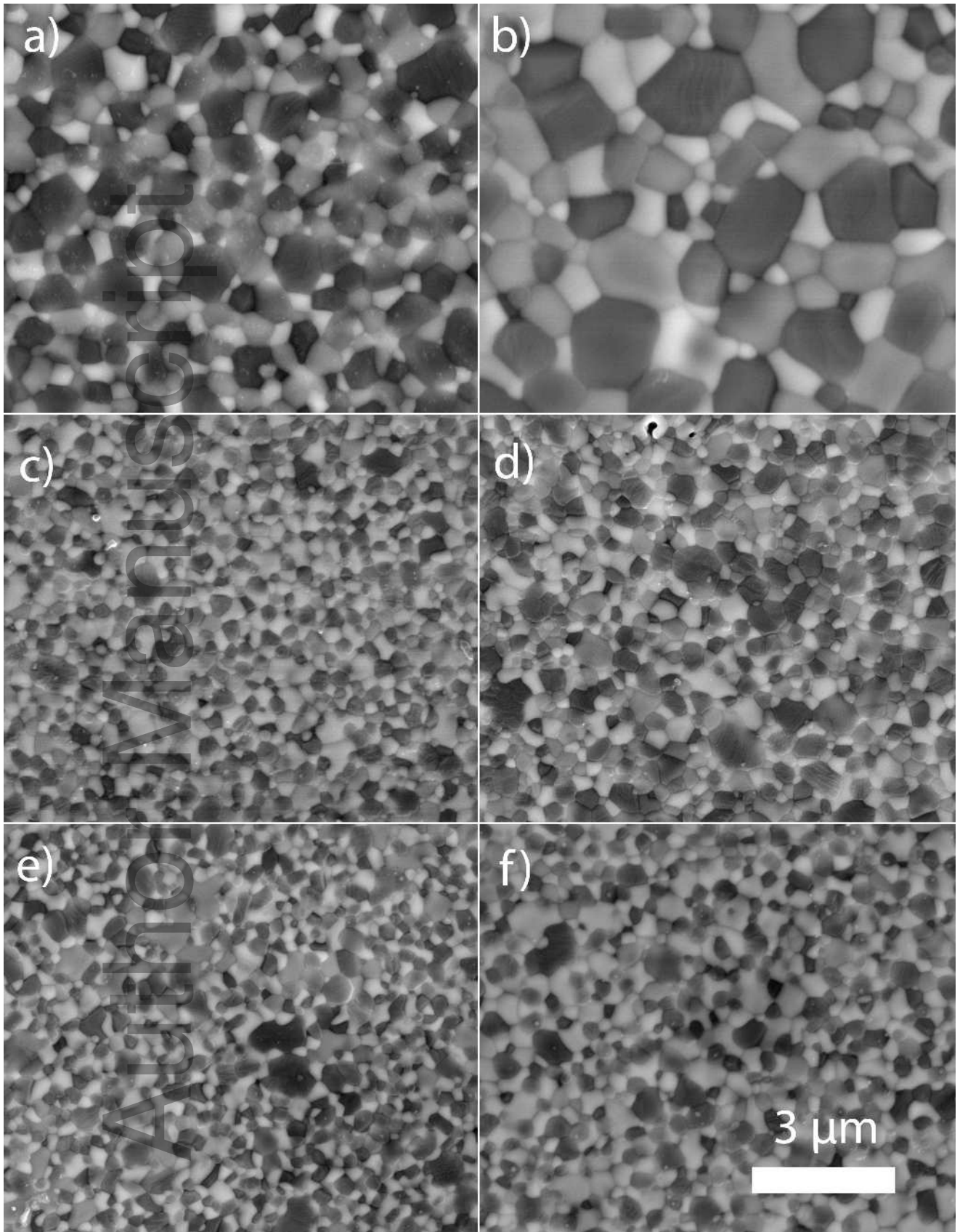jace_14761_f6.eps

3 μm

jace_14761_f7.tif